Computer Networks 197 (2021) 108334

Contents lists available at ScienceDirect

Computer Networks

journal homepage: www.elsevier.com/locate/comnet

Secure beamforming with nonorthogonal multiple access transmission in cooperative CR networks for Internet of Things☆

Quanzhong Li [a,b,*], Liang Yang [c]

[a] School of Computer Science and Engineering, Sun Yat-sen University, Guangzhou 510006, China
[b] GuangDong Province Key Laboratory of Information Security Technology, Guangzhou 510006, China
[c] College of Computer Science and Electronic Engineering, Hunan University, Changsha 410082, China

ARTICLE INFO

Keywords:
Internet of Things
Cognitive radio
Secure beamforming
Nonorthogonal multiple access
Optimization algorithms

ABSTRACT

In this paper, secure beamforming design in cooperative cognitive radio networks for Internet of Things (IoT) is investigated, where we maximize the secrecy sum rate for the IoT devices (IoDs) to protect their communication and employ the nonorthogonal multiple access scheme at the cognitive access point (AP) to serve the cognitive users. The formulated secure beamforming optimization problem is a non-convex problem and its global optimal solution is very hard to find. To overcome this difficulty, we propose an iterative algorithm based on semidefinite programming and monotonic optimization method to obtain the global optimal solution, which has high computational complexity and is suitable for the case that the cognitive AP has a powerful computing ability. For some application scenarios in which the cognitive AP has a lower computing ability, we propose suboptimal solutions based on zero-forcing scheme, which have much lower computational complexity. Furthermore, we derive the limit value of the secrecy sum rate for the IoDs when the transmit power of the cognitive AP goes to infinity, which can serve as an upper bound for our proposed solutions. Numerical results are also provided to verify the effectiveness of our proposed solutions.

1. Introduction

Internet of Things (IoT) is a powerful information technology to connect an enormous amount of devices to build a smart world [1–3]. With a rapid development of wireless technique, more and more IoT devices (IoDs) exchange information between them through wireless networks, which raises a huge demand of wireless spectrum resources. Unfortunately, available wireless spectrum resources are very limited and thus cause the spectrum resource scarcity problem for IoT applications and developments.

Cognitive radio (CR) is a promising technique for easing the strain on the spectrum resources [4]. Many works have be done by employing CR for IoT applications [5–7], where the spectrum sharing is a key issue. Usually, there are three methods for spectrum sharing, i.e., overlay method, underlay method, and interweave method [8]. In overlay method, cooperative CR is a new diagram for spectrum sharing, in which the cognitive access point (AP) works as a relaying station and assists the primary users to transmit their signals, and as a return, the cognitive AP can use the spectrum occupied by the primary users to serve its own cognitive users (CUs). By this cooperative CR diagram, the spectrum utilization is significantly improved [8].

Apart from improving the spectrum utilization, it also needs other technique to improve the spectrum efficiency for IoT applications, which is characterized by information rate or system capacity. Nonorthogonal multiple access (NOMA) is an effective and new technique over conventional orthogonal multiple access to enhance the spectrum efficiency, through transmitting the superposition of the weighted version of the strong (central) and weak (edge) users' signals and employing successive interference cancellation (SIC) at the strong user [9–13]. Power domain NOMA is the most commonly used [14–16] and many works have investigated using NOMA scheme to improve the spectrum efficiency for IoT applications [17–23]. There have been also a few works to study CR networks with NOMA scheme for IoT applications [24–27]. In [24], cognitive industrial IoT has been proposed to improve spectrum utilization by exploiting the idle spectrum, where the nodes transmit via NOMA scheme to enhance their information rates. In [25], the authors study the end-to-end outage probability

☆ This work was supported in part by the National Natural Science Foundation of China under Grant 61802447, and in part by the Hunan Natural Science Foundation, China under Grant 2019JJ40043.

* Corresponding author at: School of Computer Science and Engineering, Sun Yat-sen University, Guangzhou 510006, China.
E-mail addresses: liquanzh@mail.sysu.edu.cn (Q. Li), liangy@hnu.edu.cn (L. Yang).

https://doi.org/10.1016/j.comnet.2021.108334
Received 8 January 2021; Received in revised form 25 April 2021; Accepted 13 July 2021
Available online 21 July 2021

for the secondary NOMA users of underlay CR NOMA enabled IoT networks. In [26], a downlink robust resource allocation algorithm is proposed to maximize the sum energy efficiency of secondary users in an underlay cognitive NOMA IoT network. In [27], the authors focus on the energy-efficient optimization of an underlay cognitive multiple-input single-output NOMA IoT system with the aid of simultaneous wireless information and power transfer.

Although wireless connection is a convenient and effective method to exchange information in IoT, it also faces information security problem, since wireless information is likely to be intercepted by potential eavesdroppers due to the free propagation of wireless signals. To ensure information security, physical layer security (PLS) communication is an effective method [28–30], and has been widely adopted for IoT [31–41], where the security performance is determined by the achievable secrecy rate of the network. It has been shown in [31–41] that employing beamforming design for IoT can significantly enlarge the secrecy rate and thus improve the security performance. The works [31–40] consider non-CR network settings for IoT and [41] investigates CR network settings, where simple beamforming technique such as zero-forcing (ZF) beamforming [31–34], maximal-ratio-transmission (MRT) beamforming [33–37] or suboptimal beamforming schemes [38–41] are proposed.

It has been shown in [24–27] that combining CR networks with NOMA scheme for IoT applications can improve the information rate of IoDs significantly, which means that the secrecy sum rate of IoDs can be enhanced by employing CR combining with NOMA scheme, since the secrecy sum rate is the difference of the information rate of IoDs and eavesdroppers. To achieve this target, two main challenges are needed to deal with. One is that we need to choose a proper operation mode between the cognitive AP and the IoDs, which may have a great impact on the security performance. For example, if the underlying mode is adopted as in [25–27], the transmit power of the cognitive AP will be very limited because the interference from the cognitive AP to the IoDs cannot exceed the given threshold, and thus small secrecy sum rate of IoDs will be expected. The other challenge is with NOMA transmission, the SIC is performed at the strong CU and to ensure the success of SIC, non-convex constraints of information rate are added. Furthermore, the optimization objective (i.e., the secrecy sum rate) is also a non-convex function. These make the security optimization problem being a non-convex problem and thus it becomes a hard work to improve security performance without effective optimization algorithms. To the best of our knowledge, there is still no research on security optimization design for CR IoT networks with NOMA transmission.

In this paper, we investigate the PLS optimization for CR IoT networks with NOMA transmission and propose a cooperative CR mode, where two IoDs exchange information to each other with the help of a multi-antenna cognitive AP, and the cognitive AP employs NOMA scheme to serve its two CUs. The central CU is considered to be a potential eavesdropper with interest in the information of the IoDs, for that it is near to the cognitive AP and more likely to decode the signals of the IoDs successfully than the edge CU. We aim to design optimal beamforming to improve the PLS of the network. We first formulate the secure beamforming optimization problem, which is a non-convex problem. Then we propose several effective optimization solutions for this non-convex optimization problem, considering both optimization quality and computation complexity. We also verify the proposed optimization solutions through extensive simulations. The main contributions of this paper are summarized as follow.

- We propose a cooperative CR network with NOMA transmission for IoT applications, and formulate a secure beamforming optimization problem for ensuring the information security.
- To solve the secure beamforming optimization problem globally, we propose a semidefinite programming (SDP) [42] and monotonic optimization (MO) [43] method based iterative algorithm, which can converge to a global optimal solution and has high complexity.
- In order to adapt to the cognitive AP with lower computing abilities, we also propose suboptimal solutions based on ZF scheme, whose complexity is much lower than that of the global optimal solution.
- We derive the limit value of the secrecy sum rate for IoDs when the transmit power of the cognitive AP goes to infinity, which can serve as an upper bound or a performance reference for the proposed optimization solutions.

Note that our work is very different from the previous works in [31–41]. First, we provide a global optimal solution for the non-convex secure beamforming optimization problem while only simple or suboptimal beamforming for PLS communications are proposed in [31–41]. Second, we derive the limit value of the secrecy sum rate which can serve as an upper bound for the security performance while no such asymptotic performance bounds are provided in [31–41]. Third, we introduce CR networks for IoT applications to relieve spectrum tension while the works [31–40] consider non-CR settings. Last, we employ NOMA transmission in IoT to improve spectrum efficiency while conventional orthogonal multiple access is adopted in [31–41].

The remaining parts of this paper are organized as follows. In Section 2, the system model for a cooperative CR network for IoT is described, and the secure beamforming optimization problem is formulated. In Section 3, we propose the SDP and MO method based global optimal solution. In Section 4, we propose low-complexity suboptimal solutions based on ZF scheme. In Section 5, we derive the limit value of the secrecy sum rate for IoDs when the transmit power of the cognitive AP goes to infinity. We provide the numerical results in Section 6, and conclude our paper in Section 7.

The notations used in this paper are as follows. The $\mathrm{tr}(\mathbf{V})$, $\|\mathbf{V}\|$, $\mathbf{V}^{\dagger}$, $\mathbf{V}^{\top}$, $\mathbf{V}^{*}$, and $\mathbf{V}^{T}$ denote trace, Frobenius norm, conjugate transpose, orthogonal complement, conjugate, and transpose of the matrix $\mathbf{V}$, respectively. The $\otimes$ stands for Kronecker product. The $\mathrm{vec}(\mathbf{V})$ is to stack the columns of a matrix $\mathbf{V}$ into a vector. $\mathbf{V} \succ (\succeq) \mathbf{0}$ denotes $\mathbf{V}$ is positive definite(semidefinite). $[v]^{+}$ stands for $\max(0, v)$. The $u \searrow v$ denotes u decreases and approaches v.

2. System model and problem formulation

A cooperative CR network[1] for IoT with NOMA transmission is shown in Fig. 1, which consists of a primary network and a secondary network. In the primary network, there are two IoDs wanting to exchange information with each other. Usually, the IoDs operate in device-to-device (D2D) mode [15], or they communicate through an IoT controller [41]. However, when they are far from each other or the IoT controller is fully loaded, they cannot communicate with each other directly. To finish the communication, they ask the secondary network for help. As a return, the secondary network can use the spectrum occupied by the primary users to serve its own CUs. In the secondary network, there are one cognitive AP and two CUs,[2] i.e., one central CU and one edge CU. The cognitive AP helps the IoDs to send information and serves the two CUs by using NOMA scheme. We assume that the central CU is a potential eavesdropper other than the edge CU in [50], for the reason that the central CU is located near to the cognitive AP with better channel gains and when it is interested to wiretap the IoDs' signals it is much more likely to decode the IoDs' signals successfully than the edge CU.

The signal transmission procedure of the whole network is done in two time slots. In the first time slot, IoD i, $i = 1, 2$,[3] transmits the

[1] Unlike underlay CR networks where the secondary transmitter makes interference to the primary network [25–27], we consider a cooperative CR network that is a new diagram for spectrum sharing [44–46], where no interference channels [47] will occur between the primary and secondary networks.

[2] We consider two CUs in this paper. If there are more than two CUs, some pairing schemes in [48,49] can be adopted and one pair of CUs is scheduled to be served at a time.

[3] This index is omitted hereinafter for brevity.

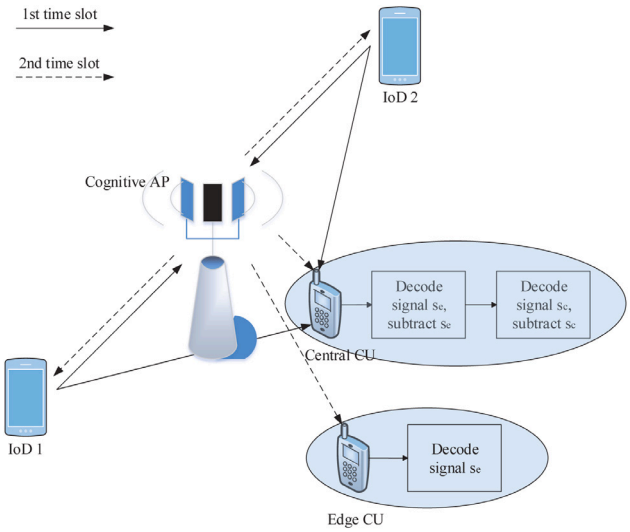

Fig. 1. The model for a CR IoT network with NOMA transmission.

information symbol s_i with $\mathbb{E}[|s_i|^2] = P_i$ to the cognitive AP. Due to the broadcast property of wireless transmission, the signal can be received at the cognitive AP and the central CU, which is given by

$$\mathbf{x}_1 = \sum_{i=1}^{2} \mathbf{h}_i s_i + \mathbf{n}_1, \tag{1}$$

and

$$x_c = \sum_{i=1}^{2} u_i s_i + n_c, \tag{2}$$

respectively, where $\mathbf{h}_i = [h_{i,1}, h_{i,2}, \ldots, h_{i,N}]^T$ denotes the channel[4] from IoD i to the cognitive AP and N is the antenna number of the cognitive AP. u_i denotes the channel from IoD i to the central CU. The entries of $\mathbf{n}_1 = [n_{1,1}, n_{1,2}, \ldots, n_{1,N}]^T$ and n_c are Gaussian noises with zero mean and variance σ^2.

In the second time slot, the cognitive AP will broadcast the signals to the IoDs, central and edge CUs. Before broadcasting, the cognitive AP multiplies the received signal $\mathbf{x}_1$ by a beamforming matrix $\mathbf{W} = [w_{i,j}]_{N,N}$ and employs NOMA scheme to transmit the information symbols s_c and s_e to the central CU and edge CU, respectively, which are also multiplied by the corresponding beamforming vector $\mathbf{w}_c = [w_{c,1}, w_{c,2}, \ldots, w_{c,N}]^T$ and $\mathbf{w}_e = [w_{e,1}, w_{e,2}, \ldots, w_{e,N}]^T$. To protect the information security of IoDs more effectively, the cognitive AP also transmits an artificial noise (AN) signal $\mathbf{z} = [z_1, z_2, \ldots, z_N]^T$ to interfere the central CU. Thus, the signal transmitted by the cognitive AP is given by

$$\mathbf{x}_2 = \mathbf{W}\mathbf{x}_1 + \mathbf{w}_c s_c + \mathbf{w}_e s_e + \mathbf{z}, \tag{3}$$

and the transmit power of the cognitive AP can be expressed as

$$P_{AP} = \mathbf{w}^\dagger \mathbf{R} \mathbf{w} + \mathbf{w}_c^\dagger \mathbf{w}_c + \mathbf{w}_e^\dagger \mathbf{w}_e + \mathrm{tr}(\mathbf{Z}), \tag{4}$$

where $\mathbf{w} = \mathrm{vec}(\mathbf{W})$, $\mathbf{R} = \mathbf{H}^T \otimes \mathbf{I}$, $\mathbf{H} \triangleq \sum_{i=1}^{2} P_i \mathbf{h}_i \mathbf{h}_i^\dagger + \sigma^2 \mathbf{I}$, and $\mathbf{Z} = \mathbb{E}\{\mathbf{z}\mathbf{z}^\dagger\}$.

Denote $\mathbf{g}_i = [g_{i,1}, g_{i,2}, \ldots, g_{i,N}]^T$, $i = 1, 2, c, e$, as the channel from the cognitive AP to IoD 1, IoD 2, central CU, and edge CU, respectively. We can express the received signal at the IoD 1, IoD 2, central CU, and edge CU as

$$y_i = \mathbf{g}_i^T \mathbf{x}_2 + n_{2,i}, \ i = 1, 2, c, e \tag{5}$$

where $n_{2,i}$ are Gaussian noises with zero mean and variance σ^2.

In the primary network, IoD i knows its own transmitted information symbol s_i, and it can subtract the self-interference term $\mathbf{g}_i^T \mathbf{W} \mathbf{h}_i s_i$ from y_i. Thus, the remaining received signal at IoD i is

$$\tilde{y}_i = \mathbf{g}_i^T (\mathbf{W}\mathbf{h}_{\hat{i}} s_{\hat{i}} + \mathbf{W}\mathbf{n}_1 + \mathbf{w}_c s_c + \mathbf{w}_e s_e + \mathbf{z}) + n_{2,i} \tag{6}$$

where $\hat{i} \triangleq 3 - i, i = 1, 2$.

According to (6), the received signal-to-interference-and-noise ratio (SINR) at IoD i is

$$\gamma_i = \frac{\mathbf{w}^\dagger \mathbf{Q}_i \mathbf{w}}{\mathbf{w}^\dagger \mathbf{R}_i \mathbf{w} + \mathbf{g}_i^T (\mathbf{w}_c \mathbf{w}_c^\dagger + \mathbf{w}_e \mathbf{w}_e^\dagger + \mathbf{Z}) \mathbf{g}_i^* + \sigma^2}, \tag{7}$$

where $\mathbf{Q}_i = P_{\hat{i}} [(\mathbf{h}_i \mathbf{h}_{\hat{i}}^\dagger) \otimes (\mathbf{g}_i \mathbf{g}_i^\dagger)]^T$, $\mathbf{R}_i = [(\sigma^2 \mathbf{I}) \otimes (\mathbf{g}_i \mathbf{g}_i^\dagger)]^T$.

In the secondary network, since the cognitive AP employs NOMA scheme to serve the central and edge CUs, the central CU near to the cognitive AP can use SIC to decode the signal of the edge CU and its own signal sequentially. The SINR to decode the signal of the edge CU at the central CU is given by

$$\gamma_{e,1} = \frac{\mathbf{w}_e^\dagger \mathbf{Q}_c \mathbf{w}_e}{\mathbf{w}^\dagger \mathbf{R}_c \mathbf{w} + \mathbf{g}_c^T (\mathbf{w}_c \mathbf{w}_c^\dagger + \mathbf{Z}) \mathbf{g}_c^* + \sigma^2}, \tag{8}$$

where $\mathbf{Q}_c \triangleq (\mathbf{g}_c \mathbf{g}_c^\dagger)^*$, $\mathbf{R}_c = [\mathbf{H} \otimes (\mathbf{g}_c \mathbf{g}_c^\dagger)]^T$.

After the central CU successfully decodes the signal of the edge CU, i.e., $\gamma_{e,1} \geq \bar{\gamma}_e$, where $\bar{\gamma}_e$ is the required SINR for decoding signals correctly, the central CU can subtract the signal of the edge CU from its received signal and then decode its own signal. Thus, the received SINR of the central CU itself is

$$\gamma_c = \frac{\mathbf{w}_c^\dagger \mathbf{Q}_c \mathbf{w}_c}{\mathbf{w}^\dagger \mathbf{R}_c \mathbf{w} + \mathbf{g}_c^T \mathbf{Z} \mathbf{g}_c^* + \sigma^2}. \tag{9}$$

At the edge CU, it decodes its signal directly by treating other signals as noises and then the received SINR of its own signal is

$$\gamma_{e,2} = \frac{\mathbf{w}_e^\dagger \mathbf{Q}_e \mathbf{w}_e}{\mathbf{w}^\dagger \mathbf{R}_e \mathbf{w} + \mathbf{g}_e^T (\mathbf{w}_c \mathbf{w}_c^\dagger + \mathbf{Z}) \mathbf{g}_e^* + \sigma^2}, \tag{10}$$

where $\mathbf{Q}_e = (\mathbf{g}_e \mathbf{g}_e^\dagger)^*$, $\mathbf{R}_e = [\mathbf{H} \otimes (\mathbf{g}_e \mathbf{g}_e^\dagger)]^T$. To ensure that the edge CU can successfully decode its own signal, it also requires that $\gamma_{e,2} \geq \bar{\gamma}_e$.

In addition, to satisfy the quality of service (QoS) requirement of the central CU, we assume that $\gamma_c \geq \bar{\gamma}_c$, where $\bar{\gamma}_c$ is the required SINR for decoding signals correctly. Thus, the central CU can also subtract the signal of its own from its received signal and try to wiretap the signals of IoDs. After subtracting, the remaining signal at the central CU with aiming to decode the signals of IoDs is given by

$$\tilde{y}_c = \mathbf{g}_c^T (\mathbf{W}\mathbf{h}_1 s_1 + \mathbf{W}\mathbf{h}_2 s_2 + \mathbf{W}\mathbf{n}_1 + \mathbf{z}) + n_{2,c}. \tag{11}$$

To obtain the largest eavesdropping information rate, the central CU combines the received signals related to IoDs at two time slots as a multiple-input-multiple-output (MIMO) channel:

$$\begin{bmatrix} x_c \\ \tilde{y}_c \end{bmatrix} = \underbrace{\begin{bmatrix} u_1 & u_2 \\ \mathbf{g}_c^T \mathbf{W}\mathbf{h}_1 & \mathbf{g}_c^T \mathbf{W}\mathbf{h}_2 \end{bmatrix}}_{\triangleq \mathbf{U}} \begin{bmatrix} s_1 \\ s_2 \end{bmatrix} + \mathbf{n} \tag{12}$$

where $\mathbf{n} = \mathrm{diag}(n_c, \mathbf{g}_c^T (\mathbf{W}\mathbf{n}_1 + \mathbf{z}) + n_{2,c})$.

According to (12), the achievable information rate for IoDs at the central CU is computed as [51]

$$R = 0.5 \log_2 \det \left(\mathbf{I} + \mathbf{U}\mathbf{P}\mathbf{U}^\dagger \mathbf{T}^{-1} \right) \tag{13}$$

where $\mathbf{P} = \mathrm{diag}(P_1, P_2)$, $\mathbf{T}_e = [\mathbf{I} \otimes (\mathbf{g}_c \mathbf{g}_c^\dagger)]^T$, $\mathbf{T} = \mathrm{diag}(\sigma^2, \ \mathbf{w}^\dagger \mathbf{T}_e \mathbf{w} + \mathbf{g}_c^T \mathbf{Z} \mathbf{g}_c^* + \sigma^2)$.

After some simple computations, (13) can be simplified as

$$R = 0.5 \log_2 (1 + \rho + \gamma) \tag{14}$$

where

$$\gamma = \frac{\mathbf{w}^\dagger \mathbf{Q} \mathbf{w}}{\mathbf{w}^\dagger \mathbf{T}_e \mathbf{w} + \mathbf{g}_c^T \mathbf{Z} \mathbf{g}_c^* + \sigma^2}, \tag{15}$$

[4] In this paper, we assume that the channels are flat Rayleigh block fading channels which remain constant during one time slot and change randomly from one time slot to another [23], and they can be estimated at the AP or fed back to the AP by CUs.

and $\rho \triangleq (P_1|u_1|^2 + P_2|u_2|^2)/\sigma^2$, $\mathbf{t}_i = \mathrm{vec}(\mathbf{g}_c\mathbf{h}_i^T)$, $\mathbf{Q} = 1/\sigma^2 \sum_{i=1}^{2}[(P_i P_{\hat{i}}|u_{\hat{i}}|^2 + P_i\sigma^2)\mathbf{t}_i\mathbf{t}_i^\dagger - P_i P_{\hat{i}} u_i u_{\hat{i}}^* \mathbf{t}_i^* \mathbf{t}_{\hat{i}}^T]$.

Based on (7) and (14), the achievable secrecy sum rate R_s for IoDs is given by [11,17]

$$R_s = [0.5\log_2(1+\gamma_1) + 0.5\log_2(1+\gamma_2) - 0.5\log_2(1+\beta+\gamma)]^+. \tag{16}$$

In this paper, we aim to protect the communication of IoDs and meanwhile satisfy the QoS requirements of the central and edge CUs, through designing the optimal beamforming vectors/matrix $\mathbf{w}$, $\mathbf{w}_c$, $\mathbf{w}_e$, and $\mathbf{Z}$. Thus, based on (4), (8)–(10), and (16), we formulate the secure beamforming optimization problem[5] with NOMA transmission in cooperative CR networks for IoT as

$$\max_{\mathbf{w},\mathbf{w}_c,\mathbf{w}_e,\mathbf{Z}} \quad R_s \tag{17a}$$

$$\text{s.t.} \quad \gamma_c \geq \bar{\gamma}_c, \tag{17b}$$

$$\gamma_{e,i} \geq \bar{\gamma}_e, \ i = 1,2 \tag{17c}$$

$$P_{AP} \leq P_{\max}, \tag{17d}$$

where $P_{\max}$ denotes the maximum transmit power of the cognitive AP.

3. Global optimal solution

Because of non-convex objective (17a) and constraints (17b), (17c), the secure beamforming optimization problem (17) is non-convex. Thus, it is a very difficult task to find the global optimal solution for problem (17).

The current state of the art techniques for handling the secrecy sum rate optimization problem like (17) are two optimization frameworks. One is the semidefinite relaxation (SDR) framework, where Gaussian randomization technique [52], penalty function method [53], or minorization–maximization (MM) approach [54] are employed to generate feasible suboptimal solutions. The other is the difference of convex (DC) programming framework, where the sequential parametric convex approximation (SPCA) method [55,56] or constrained concave convex procedure (CCCP) [41] are used to obtain local optimal solutions. However, all these techniques cannot find the global optimal solution for problem (17), and only suboptimal or local optimal solutions are obtained. Therefore, in the following, we will try our best to find the global optimal solution for problem (17) by employing SDP [42] and MO method [43].

3.1. SDP transformation

Let $\mathbf{X} = \mathbf{w}\mathbf{w}^\dagger$, $\mathbf{X}_c = \mathbf{w}_c\mathbf{w}_c^\dagger$, and $\mathbf{X}_e = \mathbf{w}_e\mathbf{w}_e^\dagger$, the γ_i and γ in the objective of problem (17) can be rewritten as

$$\tilde{\gamma}_i = \frac{\mathrm{tr}(\mathbf{Q}_i\mathbf{X})}{\mathrm{tr}(\mathbf{R}_i\mathbf{X}) + \mathrm{tr}(\mathbf{g}_i^*\mathbf{g}_i^T(\mathbf{X}_c + \mathbf{X}_e + \mathbf{Z})) + \sigma^2}, \tag{18}$$

$$\tilde{\gamma} = \frac{\mathrm{tr}(\mathbf{Q}\mathbf{X})}{\mathrm{tr}(\mathbf{T}_e\mathbf{X}) + \mathrm{tr}(\mathbf{Q}_c\mathbf{Z}) + \sigma^2}, \tag{19}$$

and the constraints (17b)–(17d) can be also expressed as

$$\mathrm{tr}(\mathbf{Q}_c\mathbf{X}_c) \geq \bar{\gamma}_c(\mathrm{tr}(\mathbf{R}_c\mathbf{X}) + \mathrm{tr}(\mathbf{Q}_c\mathbf{Z}) + \sigma^2), \tag{20}$$

$$\mathrm{tr}(\mathbf{Q}_c\mathbf{X}_e) \geq \bar{\gamma}_e(\mathrm{tr}(\mathbf{R}_c\mathbf{X}) + \mathrm{tr}(\mathbf{Q}_c(\mathbf{X}_c + \mathbf{Z})) + \sigma^2), \tag{21}$$

$$\mathrm{tr}(\mathbf{Q}_e\mathbf{X}_e) \geq \bar{\gamma}_e(\mathrm{tr}(\mathbf{R}_c\mathbf{X}) + \mathrm{tr}(\mathbf{Q}_e(\mathbf{X}_c + \mathbf{Z})) + \sigma^2), \tag{22}$$

$$\mathrm{tr}(\mathbf{R}\mathbf{X}) + \mathrm{tr}(\mathbf{X}_c + \mathbf{X}_e + \mathbf{Z}) \leq P_{\max}. \tag{23}$$

Based on (18)–(23), we can equivalently transform the problem (17) into the following SDP:

$$\max_{\mathbf{X},\mathbf{X}_c,\mathbf{X}_e,\mathbf{Z}} \quad \sum_{i=1}^{2} 0.5\log_2(1+\tilde{\gamma}_i) - 0.5\log_2(1+\rho+\tilde{\gamma}) \tag{24a}$$

$$\text{s.t.} \quad (20)\text{–}(23), \tag{24b}$$

$$\mathbf{X} \succeq \mathbf{0}, \mathbf{X}_c \succeq \mathbf{0}, \mathbf{X}_e \succeq \mathbf{0}, \mathbf{Z} \succeq \mathbf{0}, \tag{24c}$$

$$\mathrm{Rank}(\mathbf{X}) = \mathrm{Rank}(\mathbf{X}_c) = \mathrm{Rank}(\mathbf{X}_e) = 1. \tag{24d}$$

Note that the rank-one constraint (24d) in SDP (24) is highly nonlinear and hard to deal with. We consider the following relaxation problem of SDP (24) by dropping the rank-one constraint (24d):

$$\max_{\mathbf{X},\mathbf{X}_c,\mathbf{X}_e,\mathbf{Z}} \quad \sum_{i=1}^{2} 0.5\log_2(1+\tilde{\gamma}_i) + 0.5\log_2(1+\rho+\tilde{\gamma})^{-1} \tag{25a}$$

$$\text{s.t.} \quad (24b), (24c). \tag{25b}$$

In the following, we focus on finding the global optimal solution to SDP (25) by MO method and show that the obtained global optimal solution has rank-one property.

3.2. MO method

We define the sets:

$$\mathcal{Y} \triangleq \{\mathbf{Y} \mid \mathbf{Y} = (\mathbf{X}, \mathbf{X}_c, \mathbf{X}_e, \mathbf{Z}) \text{ satisfies } (25b)\}, \tag{26}$$

$$\mathcal{V} \triangleq \{\mathbf{v} \mid 0 \leq v_1 \leq 1+\tilde{\gamma}_1, 0 \leq v_2 \leq 1+\tilde{\gamma}_2, 0 \leq v_3 \leq (1+\rho+\tilde{\gamma})^{-1}, \ \forall\, \mathbf{Y} \in \mathcal{Y}\}, \tag{27}$$

$$D \triangleq \{\mathbf{d} \mid d_1 \geq 1, d_2 \geq 1, d_3 \geq \tilde{\gamma}_{\min}\}, \tag{28}$$

where $\tilde{\gamma}_{\min}$ is a lower bound of $(1+\rho+\tilde{\gamma})^{-1}$, and we can equivalently rewrite SDP (25) as a MO problem [43]:

$$\max_{\mathbf{v}\in\mathcal{V}} \ \Phi(\mathbf{v}) \triangleq \sum_{i=1}^{3} 0.5\log_2 v_i \quad \text{s.t. } \mathbf{v} \in \ \mathcal{V} \cap D. \tag{29}$$

The equivalence between SDP (25) and problem (29) is easy to be verified by using the monotonic increasing property of the logarithmic function.

For the MO problem (29), its global optimal solution can be found by using the polyblock outer approximation method proposed in [43], of which the main idea is to build a nested sequence of polyblocks outer approximating $\mathcal{V} \cap D$: $\mathcal{Q}_1 \supset \mathcal{Q}_2 \supset \cdots \supset \mathcal{V} \cap D$ in such a way that $\max_{\mathbf{v}\in\mathcal{Q}_l} \Phi(\mathbf{v}) \searrow \max_{\mathbf{v}\in\mathcal{V}\cap D} \Phi(\mathbf{v})$.

Assume that $\mathcal{Q}_l$ is already obtained, according to [43], creating $\mathcal{Q}_{l+1}$ based on $\mathcal{Q}_l$ needs three steps. Firstly, directly evaluate each value of $\Phi(\mathbf{v})$ over $\mathcal{U}_l$ and pick up the maximizer of $\Phi(\mathbf{v})$ over $\mathcal{Q}_l$, i.e.,

$$\mathbf{v}_0^l = \arg\max_{\mathbf{v}\in\mathcal{U}_l} \Phi(\mathbf{v}), \tag{30}$$

where $\mathcal{U}_l$ is the proper vertex set of $\mathcal{Q}_l$ with finite elements.[6]

Secondly, compute the projection[7] of the obtained $\mathbf{v}_0^l$ in the first step on the normal set $\mathcal{V}$, i.e., $\mathbf{a}^l = \pi_{\mathcal{V}}(\mathbf{v}_0^l)$, and let

$$\mathbf{v}_i^l = \mathbf{v}_0^l - (v_{0,i}^l - a_i^l)\mathbf{e}_i, \ i = 1,2,3 \tag{31}$$

where $v_{0,i}^l$ and a_i^l is the ith entry of $\mathbf{v}_0^l$ and $\mathbf{a}^l$, respectively.

Lastly, obtain $\mathcal{U}_{l+1}$ from $\mathcal{U}_l$ by replacing the vertex $\mathbf{v}_0^l$ with three new vertices $\{\mathbf{v}_j^l\}_{j=1}^3$ and only keep the proper vertices,[8] i.e.,

$$\mathcal{U}_{l+1} = (\mathcal{U}_l \setminus \{\mathbf{v}_0^l\}) \cup \{\mathbf{v}_i^l \mid \mathbf{v}_i^l \text{ is proper}, \ i = 1,2,3\}. \tag{32}$$

[5] In this paper, we focus on the information security of IoDs by maximizing the secrecy sum rate R_s (see (16)). Since R_s is usually larger than zero, it has implicitly represented the minimum SINR requirement of IoDs through $(1+\gamma_1)(1+\gamma_2) \geq 1+\beta+\gamma$.

[6] A polyblock $\mathcal{Q}_l$ is fully determined by its proper vertex set $\mathcal{U}_l$ [43].

[7] $\pi_{\mathcal{V}}(\mathbf{v})$ is a projection of $\mathbf{v}$ on a normal set $\mathcal{V}$ if $\pi_{\mathcal{V}}(\mathbf{v}) = \lambda\mathbf{v}$ where $\lambda = \max\{\beta \mid \beta\mathbf{v} \in \mathcal{V}\}$ [43].

[8] A vertex $\mathbf{v} \in \mathcal{V}$ is called proper if there does not exist another $\mathbf{v}' \in \mathcal{V}$ such that $\mathbf{v}' \geq \mathbf{v}$ [43].

Since the proper vertex set $\mathcal{U}_{l+1}$ fully determines the polyblock $\mathcal{Q}_{l+1}$ [43], $\mathcal{Q}_{l+1}$ is obtained.

However, in the above second step, the projection $\mathbf{a}^l$ is still unknown. To implement the polyblock outer approximation algorithm, the remaining task is to compute the projection $\mathbf{a}^l$. According to [43], the projection $\mathbf{a}^l = \lambda^l \mathbf{v}_0^l$ can be computed by

$$\begin{aligned}\lambda^l &= \max\{\beta \mid \beta \mathbf{v}_0^l \in \mathcal{V}\},\\ &= \max\{\beta \mid \beta \le \min\left(\frac{1+\tilde{\gamma}_1}{v_{0,1}^l}, \frac{1+\tilde{\gamma}_2}{v_{0,2}^l}, \frac{(1+\rho+\tilde{\gamma})^{-1}}{v_{0,3}^l}\right),\\ &\qquad \forall\, \mathbf{Y} \in \mathcal{Y}\}\\ &= \max_{\mathbf{Y}\in\mathcal{Y}} \min\left(\frac{1+\tilde{\gamma}_1}{v_{0,1}^l}, \frac{1+\tilde{\gamma}_2}{v_{0,2}^l}, \frac{(1+\rho+\tilde{\gamma})^{-1}}{v_{0,3}^l}\right),\end{aligned} \tag{33}$$

which is a max–min problem and its global optimal solution can be obtained by bisection method [57].

At each step of bisection method, we need to solve the following feasibility problem:

$$\max_{\mathbf{Y}\in\mathcal{Y}} \ t \tag{34a}$$

$$\text{s.t.} \ \ \tilde{\gamma}_1 \ge t v_{0,1}^l - 1, \tag{34b}$$

$$\tilde{\gamma}_2 \ge t v_{0,2}^l - 1, \tag{34c}$$

$$\tilde{\gamma} \le (t v_{0,3}^l)^{-1} - 1 - \rho, \tag{34d}$$

where t is a given value. Note that the feasibility of problem (34) is equivalent to that the optimal value of problem:

$$\min_{\mathbf{Y}\in\mathcal{Y}} \ \tilde{\gamma}_u - \tilde{\gamma}_l((t v_{0,3}^l)^{-1} - 1 - \rho) \tag{35a}$$

$$\text{s.t.} \ \ \tilde{\gamma}_1 \ge t v_{0,1}^l - 1, \tag{35b}$$

$$\tilde{\gamma}_2 \ge t v_{0,2}^l - 1, \tag{35c}$$

is no greater than 0, where $\tilde{\gamma} \triangleq \tilde{\gamma}_u/\tilde{\gamma}_l$ (see (19)).

A key observation for the property of the solutions to problem (35) is given below.

Proposition 1. *The problem (35) is a convex SDP and its optimal solution is rank-one.*

Proof. Please see Appendix A. ■

Now, we can employ bisection method in Algorithm 1 to find the global optimal solution to the max–min problem (33). Based on Proposition 1, the obtained solution is rank-one.

Algorithm 1 The bisection method for solving problem (33)

1: **Initialize:** $t_{\min} = 0$, $t_{\max}$ by a sufficiently large value, $n = 0$, and a tolerance $\epsilon \ge 0$;
2: **Repeat:**
Let $t = \frac{t_{\min}+t_{\max}}{2}$;
Solve SDP (35) by CVX [58] to obtain the optimal value η and the optimal solution $\mathbf{Y}^o$;
If $\eta \le 0$
$t_{\min} = t$;
Else
$t_{\max} = t$;
End
$n := n + 1$;
3: **Until:** $t_{\max} - t_{\min} \le \epsilon$.

After computing the projection $\mathbf{a}^l = \lambda^l \mathbf{v}_0^l$, following the steps of Algorithm 1 in [43], we can implement the polyblock outer approximation method for solving the MO problem (29) in Algorithm 2.

Algorithm 2 The MO method for solving problem (29)

1: **Initialize:** $\mathcal{U}_0 = \{\mathbf{d}_0\}$, $CBV = -\infty$, $l = 0$, and a tolerance $\xi \ge 0$;
2: **Repeat:**
Step 1. Find $\mathbf{v}_0^l$ by (30);
Step 2. Use Algorithm 1 to obtain λ^l and $\mathbf{Y}^o$;
Step 3. Compute $\mathbf{a}^l = \lambda^l \mathbf{v}_0^l$. If $\mathbf{a}^l \in \mathcal{D}$ and $\Phi(\mathbf{a}^l) > CBV$, then $CBV = \Phi(\mathbf{a}^l)$, $\mathbf{v}^o = \mathbf{v}^l$;
Step 4. Compute $\mathcal{U}_{l+1}$ by (32), and remove from $\mathcal{U}_{l+1}$ any $\mathbf{v}_i \in \mathcal{U}_{l+1}$ satisfying $\Phi(\mathbf{v}_i) < CBV + \xi$;
Step 5. $l := l + 1$;
3: **Until:** $\mathcal{U}_l = \emptyset$, i.e., $\mathcal{U}_l$ being an empty set.

Proposition 2. *Algorithm 2 converges to the global optimal solution of problem (17).*

Proof. According to Theorem 1 in [43], Algorithm 2 converges to the global optimal solution of the MO problem (29). From Proposition 1, the obtained solution by Algorithm 2 is rank-one, which means that the relaxation of problem (17) (i.e., problem (29)) is tight and there is no optimization performance loss, therefore Algorithm 2 converges to the global optimal solution of problem (17). ■

Remark 1 (*Complexity of Global Optimal Solution*)**.** The main computational burden of the proposed global optimal solution (i.e., Algorithm 2) is from solving SDP (35), whose complexity is $\mathcal{O}((mn^{3.5} + m^2n^{2.5} + m^3n^{0.5}) \cdot \log(1/\varepsilon))$, where n is the dimension of the matrix variable, m is the number of constraints, and ε is a given tolerance [42]. For SDP (35), $m = 6$ and $n = N^2$. Therefore, the complexity of solving SDP (35) is about $\mathcal{O}(N^7 \cdot \log(1/\varepsilon))$, which results in the complexity of Algorithm 2 is about $\mathcal{O}(N^7 \cdot L_1 \cdot L_2 \cdot \log(1/\varepsilon))$ where L_1 and L_2 is the iterative number for the convergence of bisection method (i.e., Algorithm 1) and Algorithm 2, respectively.

4. Low-complexity suboptimal solutions

The global optimal solution proposed in the above section has two layer iterations, and thus has high computational complexity. The global optimal solution is suitable to be implemented in some powerful cognitive AP, such as a base station or femtocell. However, in some application scenarios where the cognitive AP has lower computing ability, e.g., a laptop, the high-complexity global optimal solution is not suitable again. Thus, in this section, we propose some low-complexity suboptimal solutions.

The main idea to build the low-complexity suboptimal solutions is to employ ZF scheme, where we eliminate the interferences between IoDs and CUs and the interferences between the central CU and edge CU. Firstly, we eliminate the interferences to CUs from the signals of IoDs, that is, let

$$\mathbf{g}_c^T \mathbf{W} = \mathbf{0}, \tag{36}$$

$$\mathbf{g}_e^T \mathbf{W} = \mathbf{0}, \tag{37}$$

which lead to $\gamma = 0$. Therefore, no AN signal transmitted by the cognitive AP is needed, i.e., $\mathbf{Z} = \mathbf{0}$.

Next, we eliminate the interferences to IoDs from the signals of CUs, i.e.,

$$\mathbf{g}_i^T \mathbf{w}_c = 0, \ i = 1, 2, \tag{38}$$

$$\mathbf{g}_i^T \mathbf{w}_e = 0, \ i = 1, 2. \tag{39}$$

Lastly, we eliminate the interferences to the edge CU from the signal of the central CU, i.e.,

$$\mathbf{g}_e^T \mathbf{w}_c = 0. \tag{40}$$

Applying (36)–(40) to (17), problem (17) is decoupled into two optimization subproblems, of which the first one is

$$\min_{\mathbf{w}_c,\mathbf{w}_e} \ \mathbf{w}_c^\dagger \mathbf{w}_c + \mathbf{w}_e^\dagger \mathbf{w}_e, \tag{41a}$$

$$\text{s.t.} \ \frac{\mathbf{w}_c^\dagger \mathbf{Q}_c \mathbf{w}_c}{\sigma^2} \geq \bar{\gamma}_c, \tag{41b}$$

$$\frac{\mathbf{w}_e^\dagger \mathbf{Q}_e \mathbf{w}_e}{\sigma^2} \geq \bar{\gamma}_e, \tag{41c}$$

$$\frac{\mathbf{w}_e^\dagger \mathbf{Q}_c \mathbf{w}_e}{\mathbf{g}_c^T \mathbf{w}_c \mathbf{w}_c^\dagger \mathbf{g}_c^* + \sigma^2} \geq \bar{\gamma}_e, \tag{41d}$$

(38)–(40). (41e)

Let $\mathbf{G}_c = [\mathbf{g}_1 \ \mathbf{g}_2 \ \mathbf{g}_e]^T$, $\mathbf{G}_e = [\mathbf{g}_1 \ \mathbf{g}_2]^T$, then the constraints (38)–(40) in problem (41) are equivalent to

$$\mathbf{w}_c = \mathbf{G}_c^\top \tilde{\mathbf{x}}_c,$$
$$\mathbf{w}_e = \mathbf{G}_e^\top \tilde{\mathbf{x}}_e, \tag{42}$$

where $\tilde{\mathbf{x}}_c$ and $\tilde{\mathbf{x}}_e$ are the vectors for optimization.

Defining $\tilde{\mathbf{X}}_c = \tilde{\mathbf{x}}_c \tilde{\mathbf{x}}_c^\dagger$ and $\tilde{\mathbf{X}}_e = \tilde{\mathbf{x}}_e \tilde{\mathbf{x}}_e^\dagger$, and applying (42) to problem (41), we can transform problem (41) into the following SDP:

$$\min_{\tilde{\mathbf{X}}_c \succeq \mathbf{0}, \tilde{\mathbf{X}}_e \succeq \mathbf{0}} \ \mathrm{tr}(\mathbf{G}_c^{\top\dagger} \mathbf{G}_c^\top \tilde{\mathbf{X}}_c) + \mathrm{tr}(\mathbf{G}_e^{\top\dagger} \mathbf{G}_e^\top \tilde{\mathbf{X}}_e) \tag{43a}$$

$$\text{s.t.} \ \mathrm{tr}(\mathbf{G}_c^{\top\dagger} \mathbf{Q}_c \mathbf{G}_c^\top \tilde{\mathbf{X}}_c) \geq \sigma^2 \bar{\gamma}_c, \tag{43b}$$

$$\mathrm{tr}(\mathbf{G}_e^{\top\dagger} \mathbf{Q}_e \mathbf{G}_e^\top \tilde{\mathbf{X}}_e) \geq \sigma^2 \bar{\gamma}_e, \tag{43c}$$

$$\mathrm{tr}(\mathbf{G}_e^{\top\dagger} \mathbf{Q}_c \mathbf{G}_e^\top \tilde{\mathbf{X}}_e) \geq \bar{\gamma}_e (\mathrm{tr}(\mathbf{G}_c^{\top\dagger} \mathbf{Q}_c \mathbf{G}_c^\top \tilde{\mathbf{X}}_c) + \sigma^2), \tag{43d}$$

$$\mathrm{Rank}(\tilde{\mathbf{X}}_c) = \mathrm{Rank}(\tilde{\mathbf{X}}_e) = 1. \tag{43e}$$

For SDP (43), its global optimal solution is obtained by solving the rank-one relaxation problem:

$$\min_{\tilde{\mathbf{X}}_c \succeq \mathbf{0}, \tilde{\mathbf{X}}_e \succeq \mathbf{0}} \ (43a) \tag{44a}$$

$$\text{s.t.} \quad (43b)\text{–}(43d), \tag{44b}$$

which is convex, and its optimal solution can be found by CVX [58].

Proposition 3. *SDPs (43) and (44) have the same global optimal solution.*

Proof. Please see Appendix B. ■

The second optimization subproblem is

$$\max_{\mathbf{w}} \ \left(1 + \frac{\mathbf{w}^\dagger \mathbf{Q}_1 \mathbf{w}}{\mathbf{w}^\dagger \mathbf{R}_1 \mathbf{w} + \sigma^2}\right)\left(1 + \frac{\mathbf{w}^\dagger \mathbf{Q}_2 \mathbf{w}}{\mathbf{w}^\dagger \mathbf{R}_2 \mathbf{w} + \sigma^2}\right) \tag{45a}$$

$$\text{s.t.} \ (36), (37), \tag{45b}$$

$$\mathbf{w}^\dagger \mathbf{R} \mathbf{w} \leq \bar{P}_{\max}, \tag{45c}$$

where $\bar{P}_{\max} = P_{\max} - \mathbf{w}_c^{o\dagger} \mathbf{w}_c^o - \mathbf{w}_e^{o\dagger} \mathbf{w}_e^o$, and $(\mathbf{w}_c^o, \mathbf{w}_e^o)$ is the optimal solution to problem (41).

Similarly, problem (45) can be equivalently rewritten as the following SDP:

$$\max_{\tilde{\mathbf{X}} \succeq \mathbf{0}, \mathrm{Rank}(\tilde{\mathbf{X}})=1} \ \frac{\mathrm{tr}(\tilde{\mathbf{Q}}_1 \tilde{\mathbf{X}})}{\mathrm{tr}(\tilde{\mathbf{R}}_1 \tilde{\mathbf{X}})} \cdot \frac{\mathrm{tr}(\tilde{\mathbf{Q}}_2 \tilde{\mathbf{X}})}{\mathrm{tr}(\tilde{\mathbf{R}}_2 \tilde{\mathbf{X}})} \tag{46}$$

where $\tilde{\mathbf{Q}}_i = \mathbf{G}^{\top\dagger}(\mathbf{Q}_i + \mathbf{R}_i + \sigma^2/\bar{P}_{\max}\mathbf{R})\mathbf{G}^\top$, $\tilde{\mathbf{R}}_i = \mathbf{G}^{\top\dagger}(\mathbf{R}_i + \sigma^2/\bar{P}_{\max}\mathbf{R})\mathbf{G}^\top$, $\mathbf{G} = \mathbf{I} \otimes [\mathbf{g}_c \ \mathbf{g}_e]^T$.

Note that the SDP (46) is non-convex. However, its global optimal solution can be found by solving the following SDP:

$$\max_{\tilde{\mathbf{X}} \succeq \mathbf{0}, \eta \in [\eta_{\min} \ \eta_{\max}]} \ \eta \mathrm{tr}(\tilde{\mathbf{Q}}_1 \tilde{\mathbf{X}}) \tag{47a}$$

$$\text{s.t.} \ \mathrm{tr}(\tilde{\mathbf{R}}_1 \tilde{\mathbf{X}}) = 1, \tag{47b}$$

$$\mathrm{tr}(\tilde{\mathbf{Q}}_2 \tilde{\mathbf{X}}) \geq \eta \mathrm{tr}(\tilde{\mathbf{R}}_2 \tilde{\mathbf{X}}), \tag{47c}$$

where $\eta_{\max}$ and $\eta_{\min}$ is the largest and smallest eigenvalue of $\tilde{\mathbf{R}}_2^{-1}\tilde{\mathbf{Q}}_2$ [59], respectively.

Proposition 4. *The SDP (46) is equivalent to the SDP (47).*

Proof. Please see Appendix C. ■

Given η in the SDP (47), it reduces to be convex. Then, the optimal solution of the SDP (47) is found by one-dimension (1-D) search over η, such as bisection search [57]. 1-D search over η needs to search the best solution iteratively and still raises relatively high complexity. To further reduce the complexity, in the following, we propose another suboptimal solution for SDP (46), which does not need iterative search and only solves two convex SDPs.

Note that $\eta_{\min} \leq \mathrm{tr}(\tilde{\mathbf{Q}}_2\tilde{\mathbf{X}})/\mathrm{tr}(\tilde{\mathbf{R}}_2\tilde{\mathbf{X}}) \leq \eta_{\max}$, and $\mu_{\min} \leq \mathrm{tr}(\tilde{\mathbf{Q}}_1\tilde{\mathbf{X}})/\mathrm{tr}(\tilde{\mathbf{R}}_1\tilde{\mathbf{X}}) \leq \mu_{\max}$, where $\mu_{\max}$ and $\mu_{\min}$ is the largest and smallest eigenvalue of $\tilde{\mathbf{R}}_1^{-1}\tilde{\mathbf{Q}}_1$, respectively. Let $\tau_1 = (\eta_{\min} + \eta_{\max})/2$ and $\tau_2 = (\mu_{\min} + \mu_{\max})/2$. We solve the following two SDPs to find two suboptimal solutions:

$$\max_{\tilde{\mathbf{X}} \succeq \mathbf{0}, \mathrm{Rank}(\tilde{\mathbf{X}})=1} \ \tau_i \frac{\mathrm{tr}(\tilde{\mathbf{Q}}_i \tilde{\mathbf{X}})}{\mathrm{tr}(\tilde{\mathbf{R}}_i \tilde{\mathbf{X}})} \tag{48a}$$

$$\text{s.t.} \ \frac{\mathrm{tr}(\tilde{\mathbf{Q}}_{\bar{i}} \tilde{\mathbf{X}})}{\mathrm{tr}(\tilde{\mathbf{R}}_{\bar{i}} \tilde{\mathbf{X}})} = \tau_i, \tag{48b}$$

for $i = 1, 2$. From Proposition 4, the SDPs (48) are equivalent to

$$\max_{\tilde{\mathbf{X}} \succeq \mathbf{0}} \ \tau_i \mathrm{tr}(\tilde{\mathbf{Q}}_i \tilde{\mathbf{X}}) \tag{49a}$$

$$\text{s.t.} \ \mathrm{tr}(\tilde{\mathbf{R}}_i \tilde{\mathbf{X}}) = 1, \tag{49b}$$

$$\mathrm{tr}(\tilde{\mathbf{Q}}_{\bar{i}} \tilde{\mathbf{X}}) = \tau_i \mathrm{tr}(\tilde{\mathbf{R}}_{\bar{i}} \tilde{\mathbf{X}}), \tag{49c}$$

for $i = 1, 2$.

The SDPs (49) are convex. Assume that the optimal solution to SDPs (49) is $\tilde{\mathbf{X}}_1^\circ$ and $\tilde{\mathbf{X}}_2^\circ$, and the optimal objective value is f_1 and f_2. If $f_1 \geq f_2$, $\tilde{\mathbf{X}}_1^\circ$ is chosen as the suboptimal solution for SDP (46); otherwise, $\tilde{\mathbf{X}}_2^\circ$ is chosen.

Remark 2 (*Complexity of Suboptimal Solutions*)**.** Since the dimension of the matrix variable in SDP (47) is $N(N-2)$, which is much higher than $N-2$ for SDP (44), the main computational burden of the proposed suboptimal solutions is from solving SDP (47), whose complexity is about $\mathcal{O}(N^{3.5}(N-2)^{3.5} \cdot \log(1/\varepsilon))$ for a given η and ε. Thus, the proposed suboptimal solution where 1-D search is used to solve SDP (47) has the complexity of about $\mathcal{O}(L \cdot N^{3.5}(N-2)^{3.5} \cdot \log(1/\varepsilon))$, where L is the search number. Similarly, the proposed suboptimal solution where SDPs (49) are solved has the complexity of about $\mathcal{O}(N^{3.5}(N-2)^{3.5} \cdot \log(1/\varepsilon))$. Thus, the complexity of the proposed suboptimal solutions is much lower than that of the global optimal solution.

5. Limit value of R_s when $P_{\max} \to \infty$

From Section 3, we can obtain the largest R_s by the proposed global optimal solution (i.e., Algorithm 2). However, we still lack a fast method to evaluate the limit value of R_s when the transmit power of the cognitive AP goes to infinity, i.e., $P_{\max} \to \infty$, which can serve as an upper bound or a performance reference for the proposed solutions, especially when $P_{\max}$ has a large value. Therefore, in this section, we derive the limit value of R_s when $P_{\max} \to \infty$.

First, we observe the following results.

Lemma 1. *When $P_{\max} \to \infty$, the constraints in problem (17) can be always satisfied.*

Proof. Please see Appendix D. ■

Lemma 2. *When $P_{\max} \to \infty$, the limit value of γ_i is*

$$\lim_{P_{\max} \to \infty} \gamma_i = \frac{P_i \|\mathbf{h}_i\|^2}{\sigma^2}. \tag{50}$$

Proof. Please see Appendix E. ■

Lemma 3. *The largest value of* $(1+\rho+\gamma)^{-1}$ *is* $(1+\rho)^{-1}$.

Proof. Since $\gamma \geq 0$, $(1+\rho+\gamma)^{-1}$ has the largest value only when $\gamma = 0$, which is satisfied by using (36). ■

Based on Lemmas 1–3, we can obtain the limit value of R_s as given below.

Proposition 5. *When* $P_{\max} \to \infty$, *the limit value of* R_s *is*

$$\lim_{P_{\max}\to\infty} R_s = 0.5\log_2[\left(1+\zeta_1\right)\left(1+\zeta_2\right)/(1+\rho)] \tag{51}$$

where $\zeta_i = P_i\|\mathbf{h}_i\|^2/\sigma^2$.

Proof. When $P_{\max} \to \infty$, from Lemma 1, the largest value of R_s in problem (17) is $0.5\log_2[(1+\gamma_{1,\max})(1+\gamma_{2,\max})]+0.5\log_2[(1+\beta+\gamma)^{-1}]_{\max}$, where $\gamma_{i,\max}$ is the maximum value of γ_i. According to Lemmas 2–3, we have the limit value of R_s is $0.5\log_2[\left(1+\zeta_1\right)\left(1+\zeta_2\right)/(1+\rho)]$. ■

6. Simulation results

In this section, we verify the effectiveness of our proposed solutions through simulations. We assume that the distance from the cognitive AP to the IoD 1, IoD 2, and the edge CU is 100 m, and that to the central CU is 50 m. The path loss factor is 3. These simulation scenarios and parameters model a typical urban microcellular and picocellular transmission environment with cell radii in the range of 100–200 meters [60–62]. Correspondingly, we can model the entries of the channels $(\mathbf{h}_i, \mathbf{g}_i, \mathbf{g}_e, u_i), i = 1, 2$, and $\mathbf{g}_c$ are independent and identically distributed complex Gaussian random variables with zero mean and variance 1 and 8, respectively. The transmit power of the IoDs is assumed to be the same, i.e., $P_1 = P_2 = P$, and all the noises have unit variance.

In the simulations, we compare the following solutions:

- The SDP and MO method based global optimal solution, i.e., Algorithm 2, denoted as "GloSol", and the proposed Algorithm 2 without AN, denoted as "GloSol-noAN".
- The ZF based low-complexity suboptimal solution where 1-D search is used to solve the SDP (47) and search the best solution iteratively, denoted as "SubIter".
- The ZF based low-complexity suboptimal solution where no iterative search is needed and two convex SDPs (49) are solved, denoted as "SubNoIter".
- The limit value of the secrecy sum rate given by (51), denoted as "LimVal".
- The ZF based noniterative suboptimal solution proposed in [41], denoted as "ZF".
- The algebraic norm-maximizing scheme proposed in [63] for solving problem (45), denoted as "ANOMAX".

Before we present their achievable security performances, we compare the complexity of the proposed algorithms through the following running times.

6.1. Running time comparison of the proposed solutions

In Table 1, we compare the average running time of the proposed solutions for one channel realization under different antenna number of the cognitive AP, where the MATLAB version is R2016a, the CVX version is 2.1, and the CPU and RAM of the computer is Intel Core i7-4790K 4.0 GHz and 8 GB. From Table 1, we can see that the "GloSol" solution needs the average running time about 11∼22 times more than the "SubIter" solution and about 185∼365 times more than the "SubNoIter" solution, which means that the suboptimal solutions have much lower computational complexity than the global optimal solution.

Table 1
Average running time (in seconds) of proposed solutions versus antenna number of cognitive AP.

	N		
	$N=4$	$N=5$	$N=6$
GloSol	130.76	169.02	265.91
SubIter	11.84	12.06	12.30
SubNoIter	0.71	0.72	0.73

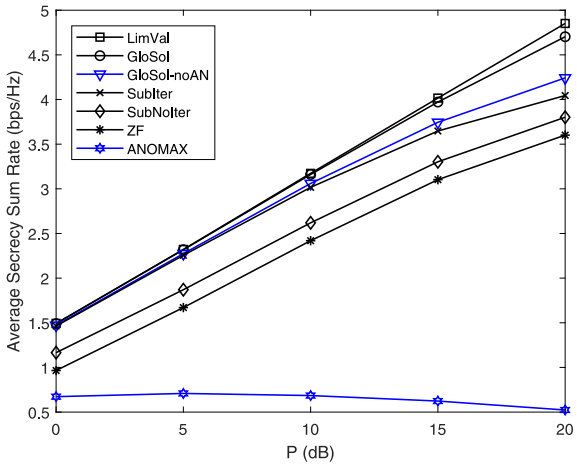

Fig. 2. Average secrecy sum rate with various solutions under different transmit power of the IoDs, P.

6.2. Average secrecy sum rate versus the transmit power of the IoDs

In Fig. 2, by changing the transmit power of the IoDs, i.e., P, we show the changes in average secrecy sum rate for IoDs, where the transmit power of the cognitive AP is $P_{\max} = 30$ dB, the SINR requirements of CUs are $\bar{\gamma}_c = 3$, $\bar{\gamma}_e = 1$, and the antenna number of the cognitive AP is $N = 4$. From Fig. 2, we can see that the proposed "GloSol" solution has the best performance and is close to the limit value of the secrecy sum rate. The proposed "GloSol-noAN" solution is worse than the "GloSol" solution, which indicates that to employ the AN can improve the security performance for IoDs. The "SubIter" solution has little performance loss compared to the "GloSol" solution when P is small. However, as P increases, the performance loss becomes larger. From Fig. 2, it is also seen that the "SubNoIter" solution has the worst performance, but it can obtain about 80% of the performance of the proposed "GloSol" solution when averaging over the transmit power of the IoDs. Furthermore, we see that the average secrecy sum rate by all the proposed solutions outperform that by the "ZF" scheme in [41] and the "ANOMAX" scheme in [63].

6.3. Average secrecy sum rate versus the transmit power of the cognitive AP

In Fig. 3, by changing the transmit power of the cognitive AP, i.e., $P_{\max}$, we show the changes in average secrecy sum rate for IoDs, where $P = 15$ dB, $\bar{\gamma}_c = 3$, $\bar{\gamma}_e = 1$, and $N = 4$. From Fig. 3, we can see that with the increase of transmit power of the cognitive AP, i.e., $P_{\max}$, average secrecy sum rate obtained by the proposed "GloSol" solution approaches the limit value. This observation indicates that as $P_{\max}$ goes to infinity, the ceiling of the secrecy sum rate occurs, since that when $P_{\max}$ goes to infinity, the secrecy sum rate depends on the transmit power of IoDs instead of $P_{\max}$ (please see Proposition 5 in Section 5). But if $P_{\max}$ is not too large, the secrecy sum rate still depends on $P_{\max}$ and grows with the increase of $P_{\max}$. From Fig. 3, we can also see that without AN, the "GloSol-noAN" solution performs worse than the "GloSol" solution, and the proposed "SubIter" solution and "SubNoIter" solution can obtain about 80% and 73% of the performance of the

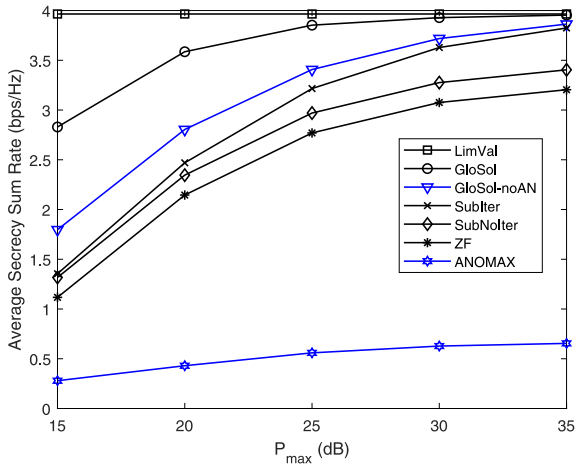

Fig. 3. Average secrecy sum rate with various solutions under different transmit power of the cognitive AP, $P_{\max}$.

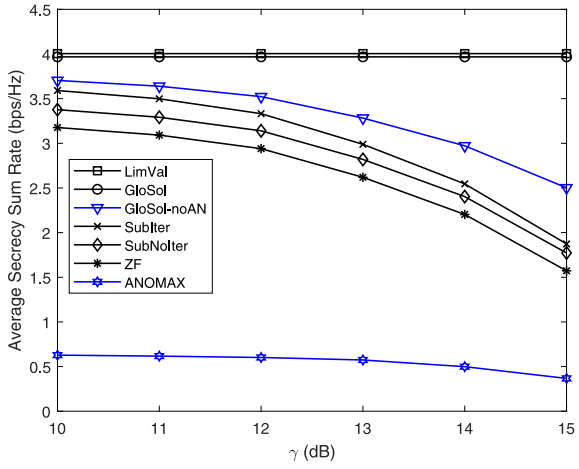

Fig. 4. Average secrecy sum rate with various solutions under different SINR requirements of CUs, where $\gamma = \bar{\gamma}_e = 0.1\bar{\gamma}_c$.

proposed "GloSol" solution when averaging over the transmit power of the cognitive AP.

6.4. Average secrecy sum rate versus the SINR requirements of CUs

In Fig. 4, by changing the SINR requirements of CUs, i.e., γ, we show the changes in average secrecy sum rate for IoDs, where $\gamma = \bar{\gamma}_e = 0.1\bar{\gamma}_c$, $P_{\max} = 30$ dB, $P = 15$ dB, and $N = 4$. From Fig. 4, we can see that the limit value of the secrecy sum rate does not change as γ increases, since it is not related with γ (see (51)). From Fig. 4, we can also see that average secrecy sum rate by the "GloSol" solution almost does not decrease with the increase of γ, since that when the transmit power of the cognitive AP is large enough and γ is not too large, the SINR requirements of CUs are always satisfied by the "GloSol" solution. However, as the SINR requirements of CUs, i.e., γ, increase, average secrecy sum rate by the "GloSol-noAN", "SubIter" and "SubNoIter" solutions becomes smaller. This is because as γ increases, more transmit power of the cognitive AP is allocated to satisfy the SINR requirements of CUs, leading to less transmit power of the cognitive AP can be used to improve the secrecy sum rate for the "SubIter" and "SubNoIter" solutions.

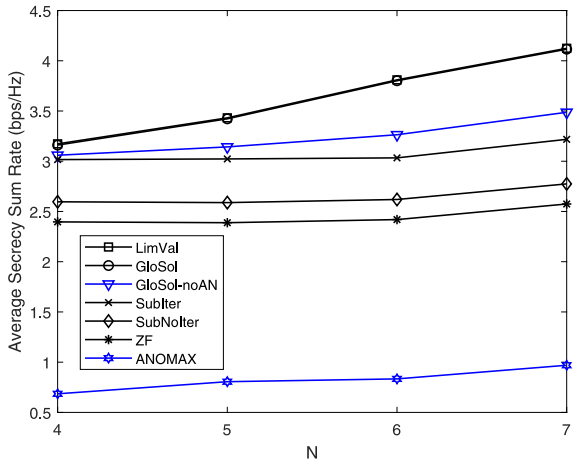

Fig. 5. Average secrecy sum rate with various solutions under different antenna number of the cognitive AP, N.

6.5. Average secrecy sum rate versus the antenna number of the cognitive AP

In Fig. 5, by changing the antenna number of the cognitive AP, i.e., N, we show the changes in average secrecy sum rate for IoDs, where $P_{\max} = 30$ dB, $P = 10$ dB, $\bar{\gamma}_c = 3$ and $\bar{\gamma}_e = 1$. From Fig. 5, we can see that as the antenna number of the cognitive AP, i.e., N, becomes larger, the average secrecy sum rate by the "GloSol", "GloSol-noAN", "SubIter", and "SubNoIter" solutions and the limit value of the secrecy sum rate also becomes larger. This can be explained as that when N becomes larger, more spatial degrees of freedom (i.e., the dimension of optimization variables) can be exploited to increase the secrecy sum rate for IoDs while satisfying the SINR requirements of CUs.

6.6. Average secrecy sum rate versus the distance from the cognitive AP to the IoDs or central CU

In Fig. 6, by changing the distance from the cognitive AP to the IoDs, i.e., d_1, we show the changes in average secrecy sum rate for IoDs, where $P_{\max} = 30$ dB, $P = 15$ dB, $\bar{\gamma}_c = 3$, $\bar{\gamma}_e = 1$, and $N = 4$. From Fig. 6, we can see that as the distance from the cognitive AP to the IoDs, i.e., d_1, increases, the average secrecy sum rate by the "GloSol", "SubIter", and "SubNoIter" solutions and the limit value of the secrecy sum rate becomes smaller. This is because the quality of the communication links between the IoDs and the cognitive AP becomes worse when d_1 increases, resulting in the decrease of secrecy sum rate.

In Fig. 7, by changing the distance from the cognitive AP to the central CU, i.e., d_2, we show the changes in average secrecy sum rate for IoDs, where $P_{\max} = 15$ or 30 dB, $P = 15$ dB, $\bar{\gamma}_c = 3$, $\bar{\gamma}_e = 1$, and $N = 4$. From Fig. 7, we can see that when $P_{\max} = 30$ dB, the average secrecy sum rate by all the proposed solutions almost does not change under different distance from the cognitive AP to the central CU, i.e., d_2. This is because when $P_{\max}$ is large, the QoS constraints are easy to be satisfied and the secrecy sum rate mainly depends on the communication links between the cognitive AP and the IoDs, irrelevant to the communication link from the cognitive AP to the central CU (please see (51) and (45a)). However, when $P_{\max} = 15$ dB, the average secrecy sum rate by the "GloSol", "SubIter", and "SubNoIter" solutions decreases as d_2 increases, since that when $P_{\max}$ is small, more power of the cognitive AP is allocated to satisfy the QoS constraints for larger d_2, resulting in smaller secrecy sum rate.

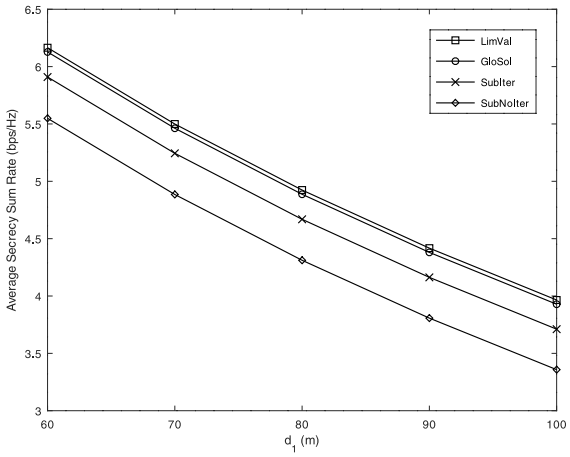

Fig. 6. Average secrecy sum rate with various solutions under different distance from the cognitive AP to the IoDs, i.e., d_1.

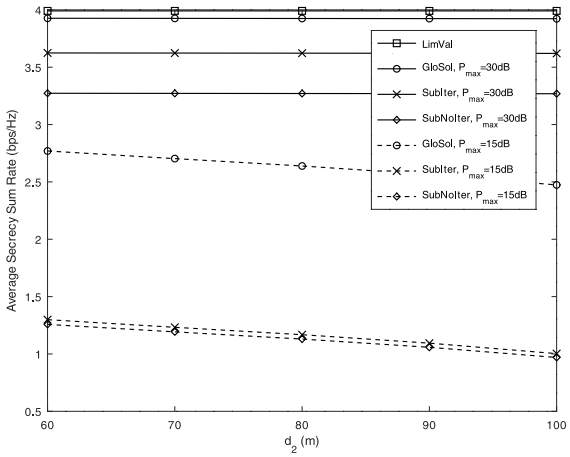

Fig. 7. Average secrecy sum rate with various solutions under different distance from the cognitive AP to the central CU, i.e., d_2.

7. Conclusions

In this paper, several optimization solutions have been proposed to maximize the secrecy sum rate for the IoDs in a cooperative CR NOMA network for IoT applications, including the SDP and MO method based global optimal solution and the ZF based suboptimal solutions, of which the latter have much lower complexity than the former and are suitable for the case that the cognitive AP is not powerful enough. We have also provided a limit value of the secrecy sum rate for the IoDs to form a performance limit for our proposed solutions. Simulation results show that the SDP and MO method based global optimal solution has the best performance and performs close to the limit value when the transmit power of the cognitive AP is sufficiently large. An interesting future work may be to employ some recent advanced techniques like reconfigurable intelligent surfaces [64–66] to further improve the security of cooperative CR NOMA networks.

Declaration of competing interest

The authors declare that they have no known competing financial interests or personal relationships that could have appeared to influence the work reported in this paper.

Appendix A. Proof of Proposition 1

Define $\tilde{\gamma}_i \triangleq \tilde{\gamma}_{i,u}/\tilde{\gamma}_{i,l}$, $i = 1, 2$ (see (18)). Then we can rewrite the SDP (35) as

$$\min_{\mathbf{Y}\in\mathcal{Y}} \ \tilde{\gamma}_u - \tilde{\gamma}_l((t\upsilon_{0,3}^l)^{-1} - 1 - \rho) \tag{52a}$$

$$\text{s.t.} \ \ \tilde{\gamma}_{i,u} \geq (t\upsilon_{0,i}^l - 1)\tilde{\gamma}_{i,l}, i = 1, 2. \tag{52b}$$

Note that the objective and constraints of (52) are all linear. Thus, the SDP (35) is convex.

Since the SDP (35) has six linear constraints, according to [67], the optimal solution $\mathbf{Y}^o = (\mathbf{X}^o, \mathbf{X}_c^o, \mathbf{X}_e^o, \mathbf{Z}^o)$ to the SDP (35) satisfies

$$\text{Rank}^2(\mathbf{X}^o) + \text{Rank}^2(\mathbf{X}_c^o) + \text{Rank}^2(\mathbf{X}_e^o) + \text{Rank}^2(\mathbf{Z}^o) \leq 6. \tag{53}$$

For the optimal $\mathbf{Y}^o$ is nonzero, we have $\text{Rank}(\mathbf{X}^o) = \text{Rank}(\mathbf{X}_c^o) = \text{Rank}(\mathbf{X}_e^o) = \text{Rank}(\mathbf{Z}^o) = 1$.

Appendix B. Proof of Proposition 3

Since SDP (44) is the rank-one relaxation of SDP (43), if the optimal solution of SDP (44) is rank-one, they have the same optimal solution. Since SDP (44) has four linear constraints, according to [67], the optimal solution $(\tilde{\mathbf{X}}_c^o, \tilde{\mathbf{X}}_e^o)$ to SDP (44) satisfies

$$\text{Rank}^2(\tilde{\mathbf{X}}_c^o) + \text{Rank}^2(\tilde{\mathbf{X}}_e^o) \leq 4. \tag{54}$$

For the optimal $(\tilde{\mathbf{X}}_c^o, \tilde{\mathbf{X}}_e^o)$ is nonzero, we have $\text{Rank}(\tilde{\mathbf{X}}_c^o) = \text{Rank}(\tilde{\mathbf{X}}_e^o) = 1$. Therefore, SDPs (43) and (44) have the same global optimal solution.

Appendix C. Proof of Proposition 4

By generalized Rayleigh quotient [59], we have

$$\max_{\tilde{\mathbf{X}}\succeq\mathbf{0},\text{Rank}(\tilde{\mathbf{X}})=1} \frac{\text{tr}(\tilde{\mathbf{Q}}_2\tilde{\mathbf{X}})}{\text{tr}(\tilde{\mathbf{R}}_2\tilde{\mathbf{X}})} = \max_{\tilde{\mathbf{w}}} \frac{\tilde{\mathbf{w}}^\dagger\tilde{\mathbf{Q}}_2\tilde{\mathbf{w}}}{\tilde{\mathbf{w}}^\dagger\tilde{\mathbf{R}}_2\tilde{\mathbf{w}}} = \eta_{\max}, \tag{55}$$

$$\min_{\tilde{\mathbf{X}}\succeq\mathbf{0},\text{Rank}(\tilde{\mathbf{X}})=1} \frac{\text{tr}(\tilde{\mathbf{Q}}_2\tilde{\mathbf{X}})}{\text{tr}(\tilde{\mathbf{R}}_2\tilde{\mathbf{X}})} = \min_{\tilde{\mathbf{w}}} \frac{\tilde{\mathbf{w}}^\dagger\tilde{\mathbf{Q}}_2\tilde{\mathbf{w}}}{\tilde{\mathbf{w}}^\dagger\tilde{\mathbf{R}}_2\tilde{\mathbf{w}}} = \eta_{\min}, \tag{56}$$

where $\eta_{\max}$ and $\eta_{\min}$ is the largest and smallest eigenvalue of $\tilde{\mathbf{R}}_2^{-1}\tilde{\mathbf{Q}}_2$, respectively.

Introducing a slack variable such that $\text{tr}(\tilde{\mathbf{Q}}_2\tilde{\mathbf{X}})/\text{tr}(\tilde{\mathbf{R}}_2\tilde{\mathbf{X}}) \geq \eta$, we equivalently transform SDP (46) into

$$\max_{\tilde{\mathbf{X}}\succeq\mathbf{0},\eta\in[\eta_{\min}\ \eta_{\max}]} \eta\frac{\text{tr}(\tilde{\mathbf{Q}}_1\tilde{\mathbf{X}})}{\text{tr}(\tilde{\mathbf{R}}_1\tilde{\mathbf{X}})} \tag{57a}$$

$$\text{s.t.} \ \ \text{tr}(\tilde{\mathbf{Q}}_2\tilde{\mathbf{X}}) \geq \eta\text{tr}(\tilde{\mathbf{R}}_2\tilde{\mathbf{X}}). \tag{57b}$$

By applying the Charnes–Cooper transformation [68], i.e.,

$$\tilde{\mathbf{Y}} = \tilde{y}\tilde{\mathbf{X}}, \ \ \tilde{y} = \frac{1}{\text{tr}(\tilde{\mathbf{R}}_1\tilde{\mathbf{X}})} \tag{58}$$

to SDP (57), we have

$$\max_{\tilde{\mathbf{Y}}\succeq\mathbf{0},\eta\in[\eta_{\min}\ \eta_{\max}]} \eta\text{tr}(\tilde{\mathbf{Q}}_1\tilde{\mathbf{Y}}) \tag{59a}$$

$$\text{s.t.} \ \ \text{tr}(\tilde{\mathbf{R}}_1\tilde{\mathbf{Y}}) = 1, \tag{59b}$$

$$\text{tr}(\tilde{\mathbf{Q}}_2\tilde{\mathbf{Y}}) \geq \eta\text{tr}(\tilde{\mathbf{R}}_2\tilde{\mathbf{Y}}), \tag{59c}$$

which is the same as SDP (47).

Appendix D. Proof of Lemma 1

Applying (38)–(40) to problem (17), the constraints (17b) and (17c) reduce to be (41b)–(41d). For any $\mathbf{w}_c \neq \mathbf{0}$ and $\mathbf{w}_e \neq \mathbf{0}$, let $f_1 = \frac{\mathbf{w}_c^\dagger\mathbf{Q}_c\mathbf{w}_c}{\bar{\gamma}_c\sigma^2}$ and $f_2 = \frac{\mathbf{w}_e^\dagger\mathbf{Q}_e\mathbf{w}_e}{\bar{\gamma}_e\sigma^2}$. It is easy to find a $\alpha > 0$ such $\alpha^2 f_1 = 1$, which means that $\alpha\mathbf{w}_c$ satisfies (41b). Now let $f_3 = \frac{\mathbf{w}_e^\dagger\mathbf{Q}_e\mathbf{w}_e}{\bar{\gamma}_e(\alpha^2\mathbf{g}_c^T\mathbf{w}_c\mathbf{w}_c^\dagger\mathbf{g}_c^* + \sigma^2)}$. It is also easy to find a $\beta > 0$ such $\beta^2 f_i \geq 1$, $i = 2, 3$, which means that $\beta\mathbf{w}_e$ satisfies (41c) and (41d). Lastly, since $P_{\max} \to \infty$, (17d) is satisfied automatically.

Appendix E. Proof of Lemma 2

Letting $\hat{\delta}_i^2 = \mathbf{g}_i^T(\mathbf{w}_c\mathbf{w}_c^\dagger + \mathbf{w}_e\mathbf{w}_e^\dagger + \mathbf{Z})\mathbf{g}_i^* + \sigma^2$, $\mathbf{c}_i^\dagger = \mathbf{g}_i^T\mathbf{W}$, and applying the matrix inverse lemma [59], we have

$$\begin{aligned}&\hat{\delta}_i^{-2}\mathbf{c}_i(\hat{\delta}_i^{-2}\sigma^2\mathbf{c}_i^\dagger\mathbf{c}_i+1)^{-1}\mathbf{c}_i^\dagger\\ =&\delta^{-2}(\mathbf{I}-(\mathbf{I}+\hat{\delta}_i^{-2}\sigma^2\mathbf{c}_i\mathbf{c}_i^\dagger)^{-1}).\end{aligned}\tag{60}$$

Further let $\mathbf{W} = \lambda\bar{\mathbf{W}}$ with $\|\bar{\mathbf{W}}\| = 1$. When $P_{\max} \to \infty$, we just let $\lambda \to \infty$. According to (60), we have

$$\begin{aligned}&\lim_{P_{\max}\to\infty}\gamma_i = \frac{P_{\hat{i}}}{\hat{\sigma}_{\hat{i}}^2}\mathbf{h}_{\hat{i}}^\dagger[\mathbf{c}_i(\hat{\delta}_i^{-2}\sigma^2\mathbf{c}_i^\dagger\mathbf{c}_i+1)^{-1}\mathbf{c}_i^\dagger]\mathbf{h}_{\hat{i}}\\ =&\lim_{\lambda\to\infty}\frac{P_{\hat{i}}}{\sigma^2}\mathbf{h}_{\hat{i}}^\dagger[(\mathbf{I}-(\mathbf{I}+\lambda^2\hat{\delta}_i^{-2}\sigma^2\mathbf{c}_i\mathbf{c}_i^\dagger)^{-1})]\mathbf{h}_{\hat{i}}\\ =&\frac{P_{\hat{i}}\|\mathbf{h}_{\hat{i}}\|^2}{\sigma^2}.\end{aligned}\tag{61}$$

References

[1] A. Al-Fuqaha, M. Guizani, M. Mohammadi, M. Aledhari, M. Ayyash, Internet of Things: A survey on enabling technologies, protocols, andapplications, IEEE Commun. Surv. Tuts. 17 (4) (2015) 2347–2376.

[2] A. Zanella, N. Bui, A. Castellani, L. Vangelista, M. Zorzi, Internet of Things for smart cities, IEEE Internet Things J. 1 (1) (2014) 22–32.

[3] L. Da Xu, W. He, S. Li, Internet of Things in industries: A survey, IEEE Trans. Ind. Inf. 10 (4) (2014) 2233–2243.

[4] S. Haykin, Cognitive radio: Brain-empowered wireless communications, IEEE J. Sel. Areas Commun. 23 (2) (2005) 201–220.

[5] Z. Yan, S. Chen, X. Zhang, H.-L. Liu, Outage performance analysisof wireless energy harvesting relay-assisted random underlay cognitivenetworks, IEEE Internet Things J. 5 (4) (2018) 2691–2699.

[6] D.S. Gurjar, H.H. Nguyen, H.D. Tuan, Wireless information and power transfer for IoT applications in overlay cognitive radio networks, IEEE Internet Things J. 6 (2) (2019) 3257–3270.

[7] Y. Liu, X. Kuai, X. Yuan, Y.-C. Liang, L. Zhou, Learning-based iterative interference cancellationfor cognitive Internet of Things, IEEE Internet Things J. 6 (4) (2019) 7213–7224.

[8] F.A. Awin, Y.M. Alginahi, E. Abdel-Raheem, K. Tepe, Technical issues on cognitive radio-based Internet of Things systems: A survey, IEEE Access 7 (2019) 97887–97908.

[9] L. Dai, et al., Non-orthogonal multiple access for 5G: Solutions, challenges, opportunities, and future research trends, IEEE Commun. Mag. 53 (9) (2015) 74–81.

[10] Z. Ding, Z. Yang, P. Fan, H.V. Poor, On the performance of nonorthogonal multiple access in 5G systems with randomly deployed users, IEEE Signal Process. Lett. 21 (12) (2014) 1501–1505.

[11] Z. Ding, J. Xu, O.A. Dobre, H.V. Poor, Joint power and timeallocation for NOMA-MEC offloading, IEEE Trans. Veh. Technol. 68 (6) (2019) 6207–6211.

[12] N. Zhao, D. Li, M. Liu, Y. Cao, Y. Chen, Z. Ding, X. Wang, Secure transmission via joint precoding optimization for downlink MISO NOMA, IEEE Trans. Veh. Technol. 68 (8) (2019) 7603–7615.

[13] Z. Yang, J.A. Hussein, P. Xu, G. Chen, Y. Wu, Z. Ding, Performance study of cognitive relay NOMA networks with dynamic power transmission, IEEE Trans. Veh. Technol. 70 (3) (2021) 2882–2887.

[14] S.M.R. Islam, N. Avazov, O.A. Dobre, K. Kwak, Power-domain non-orthogonal multiple access (NOMA) in 5G systems: Potentials and Challenges, IEEE Commun. Surv. Tuts. 19 (2) (2017) 721–742.

[15] D.-T. Do, M.-S.V. Nguyen, T.-A. Hoang, B.M. Lee, Exploiting joint base station equipped multiple antenna and full-duplex D2D users in power domain division based multiple access networks, Sensors 19 (11) (2019) 2475.

[16] D.-T. Do, M.-S.V. Nguyen, T.-A. Hoang, Exploiting secure performance in power domain based multiple access: impacts of relay link/direct link and secure analysis, Int. J. Commun. Syst. (Wiley) (2019).

[17] A. Kiani, N. Ansari, Edge computing aware NOMA for 5G networks, IEEE Internet Things J. 5 (2) (2018) 1299–1306.

[18] T. Lv, Y. Ma, J. Zen, P.T. Mathiopoulos, Millimeter-wave NOMA transmission in cellular M2M communications for Internet of Things, IEEE Internet Things J. 5 (3) (2018) 1989–2000.

[19] S. Han, X. Xu, S. Fang, Y. Sun, Y. Cao, X. Tao, P. Zhang, Energy efficient secure computation offloading in NOMA-based mMTC networks for IoT, IEEE Internet Things J. 6 (3) (2019) 5674–5690.

[20] R. Duan, J. Wang, C. Jiang, H. Yao, Y. Ren, Y. Qian, Resource allocation for multi-UAV aided IoT NOMA uplink transmission systems, IEEE Internet Things J. 6 (4) (2019) 7025–7037.

[21] A. Shahini, N. Ansari, NOMA aided narrowband IoT for machine type communications with user clustering, IEEE Internet Things J. 6 (4) (2019) 7183–7191.

[22] C.-B. Le, D.-T. Do, M. Voznak, Exploiting impact of hardware impairments in NOMA: adaptive transmission mode in FD/HD and application in Internet-of-Things, Sensors 19 (6) (2019) 1293.

[23] P. Xu, Y. Wang, G. Chen, G. Pan, Z. Ding, Design and evaluation of buffer-aided cooperative NOMA with direct transmission in IoT, IEEE Internet Things J. 8 (10) (2021) 8145–8158.

[24] X. Liu, X. Zhang, NOMA-Based resource allocation for cluster-based cognitive industrial Internet of Things, IEEE Trans. Ind. Inf. 16 (8) (2020) 5379–5388.

[25] S. Arzykulov, G. Nauryzbayev, M.S. Hashmi, A.M. Eltawil, K.M. Rabie, S. Seilov, Hardware- and interference-limited cognitive IoT relaying NOMA networks with imperfect SIC over generalized non-homogeneous fading channels, IEEE Access 8 (2020) 72942–72956.

[26] Y. Xu, R.Q. Hu, G. Li, Robust energy-efficient maximization for cognitive NOMA networks under channel uncertainties, IEEE Internet Things J. 7 (9) (2020) 8318–8330.

[27] S. Mao, S. Leng, J. Hu, K. Yang, Power minimization resource allocation for underlay MISO-NOMA SWIPT systems, IEEE Access 7 (2019) 17247–17255.

[28] Z. Xiang, W. Yang, G. Pan, Y. Cai, Y. Song, Physical layer security in cognitive radio inspired NOMA network, IEEE J. Sel. Top. Signal Process. 13 (3) (2019) 700–714.

[29] N. Nandan, S. Majhi, H. Wu, Secure beamforming for MIMO-NOMA-based cognitive radio network, IEEE Commun. Lett. 22 (8) (2018) 1708–1711.

[30] C. Huang, G. Chen, Y. Gong, Z. Han, Joint buffer-aided hybrid-duplex relay selection and power allocation for secure cognitive networks with double deep Q-network, IEEE Trans. Cogn. Commun. Net. (2021) http://dx.doi.org/10.1109/TCCN.2021.3063525.

[31] L. Hu, H. Wen, B. Wu, F. Pan, R. Liao, H. Song, J. Tang, X. Wang, Cooperative jamming for physical layer security enhancement in Internet of Things, IEEE Internet Things J. 5 (1) (2018) 219–228.

[32] J. Hu, N. Yang, Y. Cai, Secure downlink transmission in the Internet of Things: How many antennas are needed? IEEE J. Sel. Areas Commun. 36 (7) (2018) 1622–1634.

[33] H.-M. Wang, Q. Yang, Z. Ding, H.V. Poor, Secure short-packet communications for mission-critical IoT applications, IEEE Trans. Wirel. Commun. 18 (5) (2019) 2565–2578.

[34] H. Guo, Z. Yang, Y. Zou, T. Tsiftsis, M.R. Bhatangar, R.C. De Lamare, Secure beamforming for cooperative wireless-powered networks with partial CSI, IEEE Internet Things J. 6 (4) (2019) 6760–6773.

[35] A. Alsadi, S. Mohan, Improving the physical layer security of the Internet of Things (IoT), in: IEEE International Smart Cities Conference, ISC2, 2018, pp. 1–8.

[36] N. Zhang, R. Wu, S. Yuan, C. Yuan, D. Chen, RAV: Relay aided vectorized secure transmission in physical layer security for Internet of Things under active attacks, IEEE Internet Things J. 6 (5) (2019) 8496–8506.

[37] Y. Wang, T. Zhang, W. Yang, H. Yin, Y. Shen, H. Zhu, Secure communication via multiple RF-EH untrusted relays with finite energy storage, IEEE Internet Things J. 7 (2) (2020) 1476–1487.

[38] X. Hu, B. Li, K. Huang, Z. Fei, K.-K. Wong, Secrecy energy efficiency in wireless powered heterogeneous networks: a distributed ADMM approach, IEEE Access 6 (2018) 20609–20624.

[39] G. Chopra, R.K. Jha, S. Jain, Novel beamforming approach for secure communication in UDN to maximize secrecy rate and fairness security assessment, IEEE Internet Things J. 6 (4) (2019) 5935–5947.

[40] R. Rezaei, S. Sun, X. Kang, Y.L. Guan, M.R. Pakravan, S. Jain, Secrecy throughput maximization for full-duplex wireless powered IoT networks under fairness constraints, IEEE Internet Things J. 6 (4) (2019) 6964–6976.

[41] Z. Deng, Q. Li, Q. Zhang, L. Yang, J. Qin, Beamforming design for physical layer security in a two-way cognitive radio IoT network with SWIPT, IEEE Internet Things J. 6 (6) (2019) 10786–10798.

[42] A. Ben-Tal, A. Nemirovski, Lectures on Modern Convex Optimization: Analysis, Algorithms, and Engineering Applications, SIAM, Philadelphia, PA, USA, 2001, MPSSIAM Ser. Optimiz.

[43] H. Tuy, Monotonic optimization: Problems and solution approaches, SIAM J. Optim. 11 (2) (2000) 464–494.

[44] G. Zheng, S. Song, K.-K. Wong, B. Ottersten, Cooperative cognitive networks: Optimal, distributed and low-complexity algorithms, IEEE Trans. Signal Process. 61 (11) (2013) 2778–2790.

[45] J.-H. Noh, S.-J. Oh, Cognitive radio channel with cooperative multiantenna secondary systems, IEEE J. Sel. Areas Commun. 32 (3) (2014) 539–549.

[46] Q. Li, L. Yang, Beamforming for cooperative secure transmission in cognitive two-way relay networks, IEEE Trans. Inf. Forensics Secur. 15 (2020) 130–143.

[47] G.C. Alexandropoulos, C.B. Papadias, A reconfigurable iterative algorithm for the K-user MIMO interference channel, Signal Process. 93 (12) (2013) 3353–3362.

[48] X. Zhu, C. Jiang, L. Kuang, N. Ge, J. Lu, Non-orthogonal multiple access based integrated terrestrial-satellite networks, IEEE J. Sel. Areas Commun. 35 (10) (2017) 2253–2267.

[49] Z. Ding, P. Fan, H.V. Poor, Impact of user pairing on 5G nonorthogonal multiple-access downlink transmissions, IEEE Trans. Veh. Technol. 65 (8) (2016) 6010–6023.

[50] Y. Li, M. Jiang, Q. Zhang, Q. Li, J. Qin, Secure beamforming in downlink MISO nonorthogonal multiple access systems, IEEE Trans. Veh. Technol. 66 (8) (2017) 7563–7567.
[51] D. Tse, P. Viswanath, Fundamentals of Wireless Communication, Cambridge Univ. Press, Cambridge, U.K., 2005.
[52] Q. Li, Q. Zhang, J. Qin, Secure relay beamforming for SWIPT in amplify-and-forward two-way relay networks, IEEE Trans. Veh. Technol. 65 (11) (2016) 9006–9019.
[53] H. Wang, M. Luo, Q. Yin, X. Xia, Hybrid cooperative beamforming and jamming for physical-layer security of two-way relay networks, IEEE Trans. Inf. Forensics Secur. 8 (12) (2013) 2007–2020.
[54] Q. Li, W. Ma, D. Han, Sum secrecy rate maximization for full-duplex two-way relay networks using Alamouti-based rank-two beamforming, IEEE J. Sel. Top. Signal Process. 10 (8) (2016) 1359–1374.
[55] C. Wang, H. Wang, D.W.K. Ng, X. Xia, C. Liu, Joint beamforming and power allocation for secrecy in peer-to-peer relay networks, IEEE Trans. Wirel. Commun. 14 (6) (2015) 3280–3293.
[56] D. Wang, B. Bai, W. Chen, Z. Han, Secure green communication via untrusted two-way relaying: a physical layer approach, IEEE Trans. Commun. 64 (5) (2016) 1861–1874.
[57] S. Boyd, L. Vandenberghe, Convex Optimization, Cambridge Univ. Press, Cambridge, U.K., 2004.
[58] M. Grant, S. Boyd, CVX: Matlab software for disciplined convex programming, (Online), Available: http://cvxr.com/cvx.
[59] R.A. Horn, C.R. Johnson, Matrix Analysis, Cambridge Univ. Press, Cambridge, U.K., 1985.
[60] S. Rangan, T.S. Rappaport, E. Erkip, Millimeter-wave cellular wireless networks: Potentials and challenges, Proc. IEEE 102 (3) (2014) 366–385.
[61] J. Stephan, M. Brau, Y. Corre, Y. Lostanlen, Joint analysis of small-cell network performance and urban electromagnetic field exposure, in: The 8th European Conference on Antennas and Propagation, EuCAP 2014, The Hague, 2014, pp. 2623–2627.
[62] B. Pitakdumrongkija, M. Ariyoshi, L. Raschkowski, S. Jaeckel, L. Thiele, Performance evaluation of massive MIMO with low-height small-cell using realistic channel models, in: IEEE 84th Vehicular Technology Conference, VTC-Fall, Montreal, QC, 2016, pp. 1–5.
[63] F. Roemer, M. Haardt, Algebraic norm-maximizing (ANOMAX) transmit strategy for two-way relaying with MIMO amplify and forward relays, IEEE Signal Process. Lett. 16 (10) (2009) 909–912.
[64] C. Huang, A. Zappone, G.C. Alexandropoulos, M. Debbah, C. Yuen, Reconfigurable intelligent surfaces for energy efficiency in wireless communication, IEEE Trans. Wirel. Commun. 18 (8) (2019) 4157–4170.
[65] G.C. Alexandropoulos, G. Lerosey, M. Debbah, M. Fink, Reconfigurable intelligent surfaces and metamaterials: The potential of wave propagation control for 6G wireless communications, 2020, arXiv:2006.11136.
[66] L. Yang, Y. Yang, D.B. d. Costa, I. Trigui, Outage probability and capacity scaling law of multiple RIS-aided networks, IEEE Wirel. Commun. Lett. 10 (2) (2021) 256–260.
[67] Y. Huang, D.P. Palomar, Rank-constrained separable semidefinite programming with applications to optimal beamforming, IEEE Trans. Signal Process. 58 (2) (2010) 664–678.
[68] A. Charnes, W.W. Cooper, Programming with linear fractional functions, Naval Res. Logist. Q. 9 (3/4) (1962) 181–186.

Quanzhong Li received the B.S. and Ph.D. degrees from Sun Yat-sen University (SYSU), Guangzhou, China, both in information and communications engineering, in 2009 and 2014, respectively. He is currently an Associate Professor with the School of Computer Science and Engineering, SYSU. His research interests include UAV communications, non-orthogonal multiple access, wireless communications powered by energy harvesting, cognitive radio, cooperative communications, and multiple-input multiple-output communications. He is an Editor of the Mobile Information Systems.

Liang Yang was born in Hunan, China. He received the Ph.D. degree in electrical engineering from Sun Yat-sen University, Guangzhou, China, in 2006. From 2006 to 2013, he was a Teacher at Jinan University, Guangzhou. He joined the Guangdong University of Technology in 2013. He is currently a Professor at Hunan University, Changsha, China. His current research interest includes the performance analysis of wireless communications systems.